Open Research Online

The Open University's repository of research publications
and other research outputs

# Gallium-assisted diffusion bonding of stainless steel to titanium; microstructural evolution and bond strength

Journal Item

How to cite:

Shirzadi, Amir A.; Laik, Arijit; Tewari, Raghvendra; Orsborn, Jonathan and Dey, Gautam K. (2018). Gallium-assisted diffusion bonding of stainless steel to titanium; microstructural evolution and bond strength. Materialia, 4 pp. 115–126.

For guidance on citations see FAQs.

© 2018 Acta Materialia Inc.

Version: Version of Record

Link(s) to article on publisher's website:
http://dx.doi.org/doi:10.1016/j.mtla.2018.09.009

Copyright and Moral Rights for the articles on this site are retained by the individual authors and/or other copyright owners. For more information on Open Research Online's data policy on reuse of materials please consult the policies page.

oro.open.ac.uk

Materialia 4 (2018) 115–126

Contents lists available at ScienceDirect

Materialia

journal homepage: www.elsevier.com/locate/mtla

Full Length Article

# Gallium-assisted diffusion bonding of stainless steel to titanium; microstructural evolution and bond strength

Amir A. Shirzadi [a,b,*], Arijit Laik [c,d], Raghvendra Tewari [c,d], Jonathan Orsborn [e], Gautam K. Dey [c,d]

[a] School of Engineering and Innovation, The Open University, Milton Keynes MK7 6AA, UK
[b] Dongguan Centre of Excellence for Advanced Materials, Dongguan 523808, China
[c] Materials Science Division, Bhabha Atomic Research Centre, Mumbai 400 085, India
[d] Homi Bhabha National Institute, Mumbai 400 094, India
[e] Centre for Electron Microscopy and Analysis, Ohio State University, Columbus, OH 43210, USA

ARTICLE INFO

*Keywords:*
Stainless steel
Titanium
Diffusion bonding
Intermetallic
Tensile strength

ABSTRACT

Strong joints between stainless steel 304 L and pure titanium (grade-2) were made using the novel method of "*gallium-assisted diffusion bonding*". The microstructural evolution and interfacial reactions were investigated in detail. The possible mechanisms of phase changes at the joint interface when bonding with and without a nickel interlayer were identified. Layers of FeTi and $(Fe,Cr)_2Ti$ intermetallic compounds were found at the reaction zone in the case of direct bonding, whereas (Fe,Ni)Ti and $Fe_2Ti$ phases were identified in the reaction zone of the samples bonded using nickel interlayers. A layer of $\alpha$Fe was observed on the steel side of the reaction zone in both the cases, probably due to the enrichment of Cr at the interface. The diffusion of gallium led to formation of a layer of $\alpha$Ti, while the diffusion of Fe and Ni assisted in the formation of a duplex $(\alpha+\beta)$Ti phase in the inter-diffusion zone. The joints fractured along the intermetallic layers at the interface, during tensile testing, with limited ductility. The maximum tensile strengths of the bonded samples were 280 and 313 MPa with and without nickel interlayer, respectively. The latter equals 92% of the tensile strength of the pure grade-2 titanium used in this work (i.e. 340 MPa).

## 1. Introduction

Dissimilar-metal joining (DMJ), where two different metals or alloys are joined together, has been an area of active research [1]. Dissimilar joints can exploit the advantageous properties of two different materials in one component, hence they have vast applications in variety of fields, such as thermal power stations, nuclear and petrochemical plants, cryogenic vessels, micro-electronics, and medical devices [1]. However, because of several unsolved issues, such as, weakening of the joint due to difference in the thermo-physical properties of the joining materials and/or chemical incompatibilities that lead to formation of brittle intermetallic phases, DMJ has been researched extensively [2]. Among the various applications of DMJ, joining of titanium to stainless steel (Ti-SS) offers variety of applications ranging from nuclear power plants, cryogenic vessels to chemical industries [3]. One of the most critical applications of Ti-SS joints is in nuclear fuel plants, particularly in the dissolvers used for reprocessing of spent nuclear fuel [4–8].

In the context to joining of Ti to SS, fusion welding has proved unsuccessful due to the uncontrolled formation of intermetallic compounds in the weld zone, as a result of excessive heat and extensive mixing of the constituents, which substantially reduces the strength of the welded joints [2]. It is generally understood that the intermetallics do not significantly embrittle the weld provided their thickness remains low. Obtaining a thin layer of intermetallic is very difficult, if not impossible, when using conventional welding processes. This is due to the high heat inputs and low cooling rates associated with fusion welding processes, which accelerate the growth rate of intermetallic compounds.

In order to circumvent the above-mentioned problems vacuum brazing using Ag-based filler alloys, have been used to join SS and Ti. The reasons for the choice of brazing over other joining techniques have already been elaborated by the authors elsewhere [3,9]. However, due to poor corrosion resistance of the brazed SS-Ti joints, their application is limited to non-corrosive and/or low temperature environments. This drawback, to a large extent, can be overcome by adopting solid state bonding methods, such as explosive welding, friction welding and diffusion bonding. Mudali et al. [6] have reported that SS-Ti joints produced by friction welding exhibited poor bendability and corrosion resistance. Even though explosion welding has been used to clad Ti to SS plates in

* Corresponding author at: School of Engineering and Innovation, The Open University, Milton Keynes MK7 6AA, UK.
*E-mail address:* a.shirzadi@open.ac.uk (A.A. Shirzadi).

https://doi.org/10.1016/j.mtla.2018.09.009
Received 25 May 2018; Received in revised form 7 September 2018; Accepted 8 September 2018
Available online 12 September 2018
2589-1529/© 2018 Acta Materialia Inc. Published by Elsevier Ltd. This is an open access article under the CC BY license.
(http://creativecommons.org/licenses/by/4.0/)

**Table 1**
Chemical composition of the base materials (in weight percent).

| Elements | C | H | O | Mn | Si | Ni | Cr | Fe | Ti |
|---|---|---|---|---|---|---|---|---|---|
| Ti-Grade 2 | 0.009 | 0.008 | 0.12 | – | – | 0.011 | – | 0.09 | bal. |
| Stainless steel 304L | 0.02 | – | – | 1.47 | 0.52 | 10.6 | 19.1 | bal. | – |

many applications [10–13], recent reports on formation of brittle intermetallics such as FeTi and $Fe_2Ti$ [14] and accumulation of considerably high residual stresses (~1000 MPa) [15] at the Ti-SS joint interface, puts the safe use of such joints into question.

Solid state diffusion bonding, which could address the aforementioned problems, has emerged as a potential solution to produce SS-Ti joints with desirable properties. However, it should be kept in mind that direct joining of SS to Ti, due to limited mutual solubility of Fe and Ti, results in the formation of various intermetallic compounds (IMC) such as FeTi and $Fe_2Ti$ [16–19]. Most of these IMCs are brittle in nature and impair the mechanical properties of the joints. Ghosh and Chatterjee [20] reported the formation of $\sigma$-phases, FeTi, $Fe_2Ti_4O$, $Fe_2Ti$, NiTi, $NiTi_2$ and $Cr_2Ti$ in the reaction zone of commercially pure Ti (CP-Ti) and SS 304, diffusion bonded between 800 to 950 °C. They also concluded that the presence of these IMCs led to a low tensile strength of 242 MPa (i.e. 76% tensile strength of the parent CP-Ti).

To reduce the formation of brittle IMCs, use of interlayers, compatible with both SS and Ti, has proven to be beneficial. Kundu and Chatterjee [21] showed that in solid-state diffusion bonding of CP-Ti to SS 304 below 850 °C, the interface was free from reaction products when a Ni interlayer was used. However, with temperatures exceeding 900 °C, new phases, e.g. $\lambda$, $\chi$, $\alpha$Fe, FeTi, started appearing in the diffusion zone. The maximum tensile strength obtained in this case was 270 MPa for joints made at 850 °C. In a more recent work, Deng et al. [22] have demonstrated that a thin layer of Ag can be used to prevent the formation of brittle IMCs between SS 304 and Ti. They have reported that the average tensile strength of the joints ranged between 404 and 411 MPa for corresponding bonding temperatures of 825–875 °C. Use of pure Cu as an interlayer, was also found to be beneficial when bonding SS to Ti. Kundu et al. [23] have shown that solid-state diffusion bonding of CP-Ti with SS 304 using a 300 μm Cu interlayer yielded a maximum bond strength of 318 MPa with 8.5% ductility when processed at 900 °C. For bonding temperatures above 900 °C, the interface showed formation of Fe–Cu–Ti based ternary IMCs in the reaction zone. Use of Al as an interlayer provided limited success due the formation of hard aluminides at the interface [24]. It should be noted that use of such ductile interlayers assists in relieving the residual stresses that are generated at the interface upon cooling, due to the mismatch in the coefficients of thermal expansion of SS and Ti. Nevertheless, due to the presence of unreacted Ag, Al and Cu, the corrosion resistance of such joints is expected to be very poor and hence their very limited applications.

One of the common problems encountered in diffusion bonding of most metals and alloys is the presence of oxide layers on the mating surfaces, which hinder the formation of metal-to-metal contact at the joint interface. This obstacle is more relevant to the alloys and metals with stable and virtually instantaneously reforming surface oxides, e.g. Al-based alloys and Ni-based superalloys [25]. Therefore, the faying surfaces are sometimes given a surface treatment prior to bonding which assists in removing or modifying the surface oxide film. One such treatment was effectively used by Shirzadi and Wallach for joining superalloys and aluminum alloys [26,27]. This technique not only removes or modifies the continuous surface oxide film but also avoids its reformation by forming a very thin layer of gallium on the mating surfaces, thereby isolating them from the environment.

Although considerable investigation has been carried out on diffusion bonding of SS to Ti, there exists substantial scope of improving the quality of the joints by controlling the interfacial reactions. The focus of research in this frontier is primarily on the improving the joint strength by optimizing the bonding parameters and nature of interlayers. However, the main objective of the present work was to carry out an in-depth investigation on the evolution of the microstructure at the SS-Ti interface during gallium-assisted diffusion bonding, with and without using a Ni interlayer. The interfacial reactions and their mechanisms that lead to successful joining of the two materials have also been identified.

**Table 2**
Conditions used for Ga-assisted diffusion bonding of SS 304 L to Ti Grade-2.

| Sample No. | Peak Temperature ( °C) | Dwell time (min) | Interlayer |
|---|---|---|---|
| OU 10 | 1050 | 2 | – |
| OU 11 | 1050 | 20 | – |
| OU 12 | 1050 | 20 | – |
| OU 14 | 850 | 30 | – |
| OU 16 | 850 | 60 | Ni 0.8 μm |
| OU 17 | 900 | 60 | Ni 1.1μm |
| OU 18 | 800 | 60 | Ni 1.1μm |
| OU 19 | 850 | 2×30 | Ni 0.5μm |
| OU 20 | 820 | 120 | Ni 0.5μm |
| OU 21 | 820 | 60 | Ni 0.5μm |

## 2. Experimental procedure

### 2.1. Bonding process

Cylindrical blocks of austenitic stainless steel (AISI 304L) and grade-2 titanium (ASTM B265) with 22.5 mm diameter and 10 mm height were diffusion bonded in a vacuum press equipped with an induction heating system and under a vacuum level of about $5\times10^{-5}$ mbar. The nominal compositions of these materials are given in Table 1. Prior to bonding, the joining faces of the discs were ground using 1200 grade emery papers and were rinsed in acetone. The joining faces of both pieces were treated with Ga to remove the native oxide layer. This was done by grinding the faying surface with emery paper (1200 grit) containing a small amount of liquid gallium (more details are given in Ref. [27]). In one set of experiments the joining face of the SS pieces were sputter coated with 0.5–1.1 μm thick pure nickel. Diffusion bonding experiments were carried out by varying the bonding parameters, i.e. peak bonding temperature, dwell time and the thickness of interlayer, as shown in Table 2. Temperature of each sample was monitored and controlled with a k-type thermocouple spot welded on each steel block, close to the joint. Fig. 1 shows a SS-Ti diffusion bonded sample, made in 20 min at 1050 °C.

### 2.2. Characterization and evaluation

Specimens from the cross-section of the joint were prepared using standard metallographic techniques and were subsequently etched with a solution of 5% HF, 40% $HNO_3$ and 55% $H_2O$, by volume. The microstructure of the reaction zone was characterized using an optical microscope (OM), and a scanning electron microscope (SEM) equipped with an energy dispersive spectrometer (EDS). The micro-chemical analysis of the reaction products was carried out using a Cameca SX100 electron probe micro-analyser (EPMA) equipped with three wavelength dispersive spectrometers (WDS). The interfacial microstructure was also

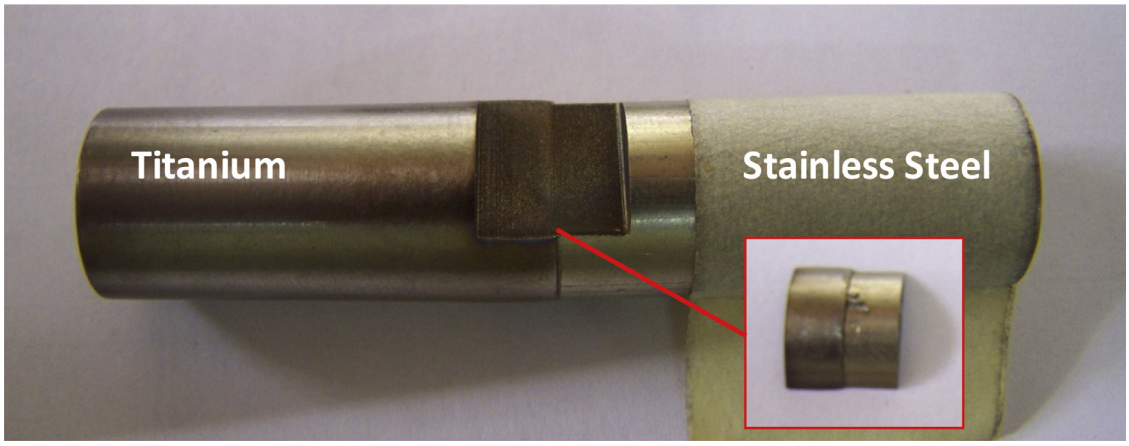


**Fig. 1.** Diffusion bonded SS-Ti joint processed at 1050 °C for 20 min. A small sample cut-off from the joint area, shown in the inset, was used for microstructural characterisation and hardness measurement.

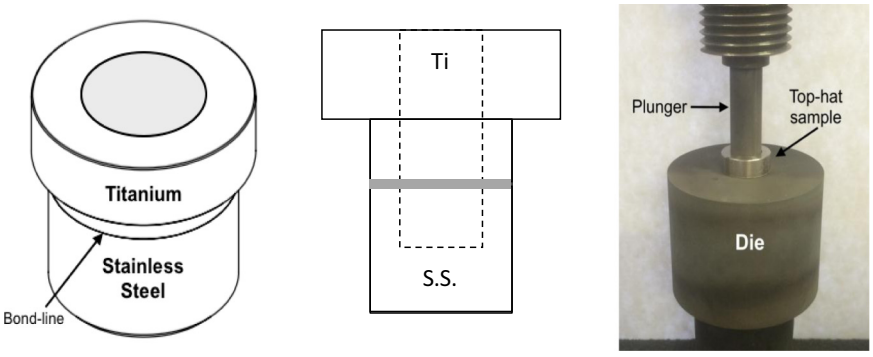


**Fig. 2.** Schematic top-hat shape sample and actual testing setup used to assess bond strength in this work.

characterized at sub-micron scale using a transmission electron microscope (TEM). The details of specimen preparation are given elsewhere [9]. The variation in hardness across the bonded cross-section was recorded using an ultra-nano-hardness tester (UNHT). The maximum load used in the indentations was only 8 mN with loading and unloading rate of 0.1 mN/s. The tensile strength of each joint was determined using a top-hat shape sample and a universal testing machine, with a cross head speed of 0.1 mm/min. Fig. 2 shows the sample and setup used for tensile testing.

**Table 3**
Chemical composition (at.%) of various phases identified on the interface of a SS-Ti sample bonded at 1050 °C for 20 min.

| Phases | Ti | Fe | Cr | Ni | Ga |
|---|---|---|---|---|---|
| $\alpha$Ti | 75.29 | 9.21 | 6.50 | 2.2 | 6.8 |
| FeTi | 52.4 | 39.4 | 2.1 | 4.7 | 1.4 |
| $Fe_2Ti$ | 34.2 | 54.4 | 8.7 | 2.4 | 0.3 |
| $\alpha$Fe | 1.5 | 65.0 | 20.8 | 7.8 | 4.9 |

## 3. Results

### 3.1. Microstructural examination of bonds without interlayer

The microstructures of all gallium bonded SS-Ti samples were found to be very similar. The optical micrograph in Fig. 3a shows a typical microstructure of the diffusion zone in the SS-Ti joint bonded at 1050 °C for 20 min. This could be taken as a representative microstructure that evolved during gallium diffusion bonding. It can be noted that the interface is free from pores, voids and discontinuities. Based on the morphological and compositional variations, the entire interaction zone could be divided into four regions namely, “A” through “D”, as marked in Fig. 3a.

Regions “A” and “B” having a combined width of about 65 µm on the Ti side, which is about one order of magnitude larger than the 7 µm wide interaction zone on the steel side (region “D” in Fig. 3a). In addition, a distinct region, marked as “C”, appeared at the interface. Fig. 3b shows a magnified view of the region “C” where two distinct phases can be seen. Based on the EDS analysis (Table 3), these phases were identified as intermetallic compounds FeTi and $Fe_2Ti$. On the SS side and in the “D” region, a layer of $\alpha$Fe was formed due to the high concentration of Cr in this region (Table 3).

Fig. 4 shows the distribution of Fe, Ni, Cr, Ti and Ga at the SS-Ti interface for a sample bonded at 1050 °C for 20 min. The elemental map of Ga showed that the entire Ga was fully diffused into the Ti and SS resulting in the formation regions “B” and “D”, respectively. The elemental maps of Fe and Ni showed that these elements have diffused into Ti up to about 100 µm depth. Deep diffusion of Fe and Ni (both $\beta$-stabilizer in Ti alloys) led to the formation of region “A” with a duplex microstructure comprising $\alpha$Ti and $\beta$Ti phases. In contrast, a single-phase region of $\alpha$Ti was found in the region “B”. As can be noted in the X-ray map of Ga in Fig. 4, the width of region "B" coincides with the extent of a high-content Ga zone in the Ti. The concentration of Ga falls abruptly across the neighbouring region “A”. Gallium is an $\alpha$-stabilising element for Ti with about 12 at.% solubility in Ti at room temperature [28]. In view of these observations, the presence of the single $\alpha$Ti phase could be attributed to the presence of Ga in the Ti. Therefore, it was inferred that $\beta$-stabilising elements such as Fe and Ni did not suppress the $\alpha$-stabilising effect of Ga. Moreover, the layer “D” on the steel side mostly

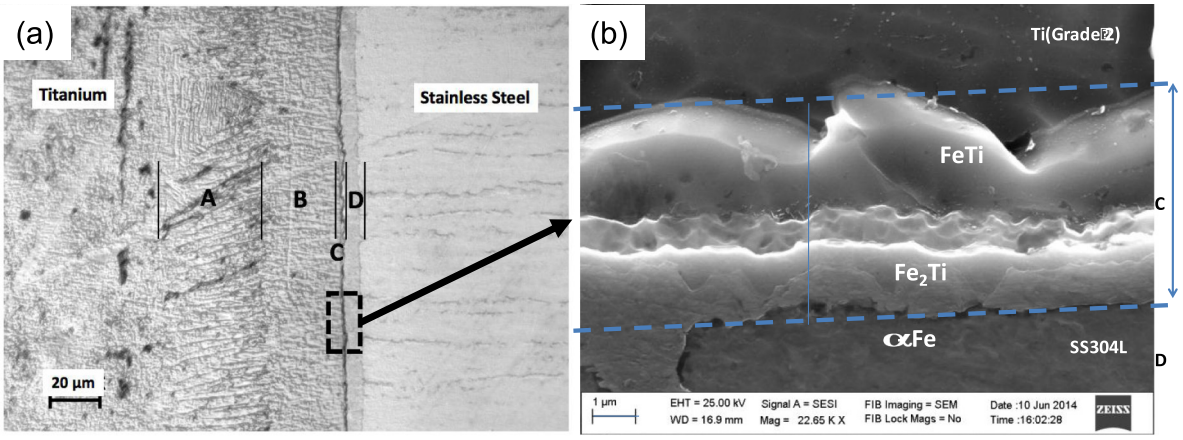


**Fig. 3.** Optical (a) and FESEM (b) micrographs of the SS-Ti interface in a sample diffusion bonded at 1050 °C for 20 min following gallium surface treatment.

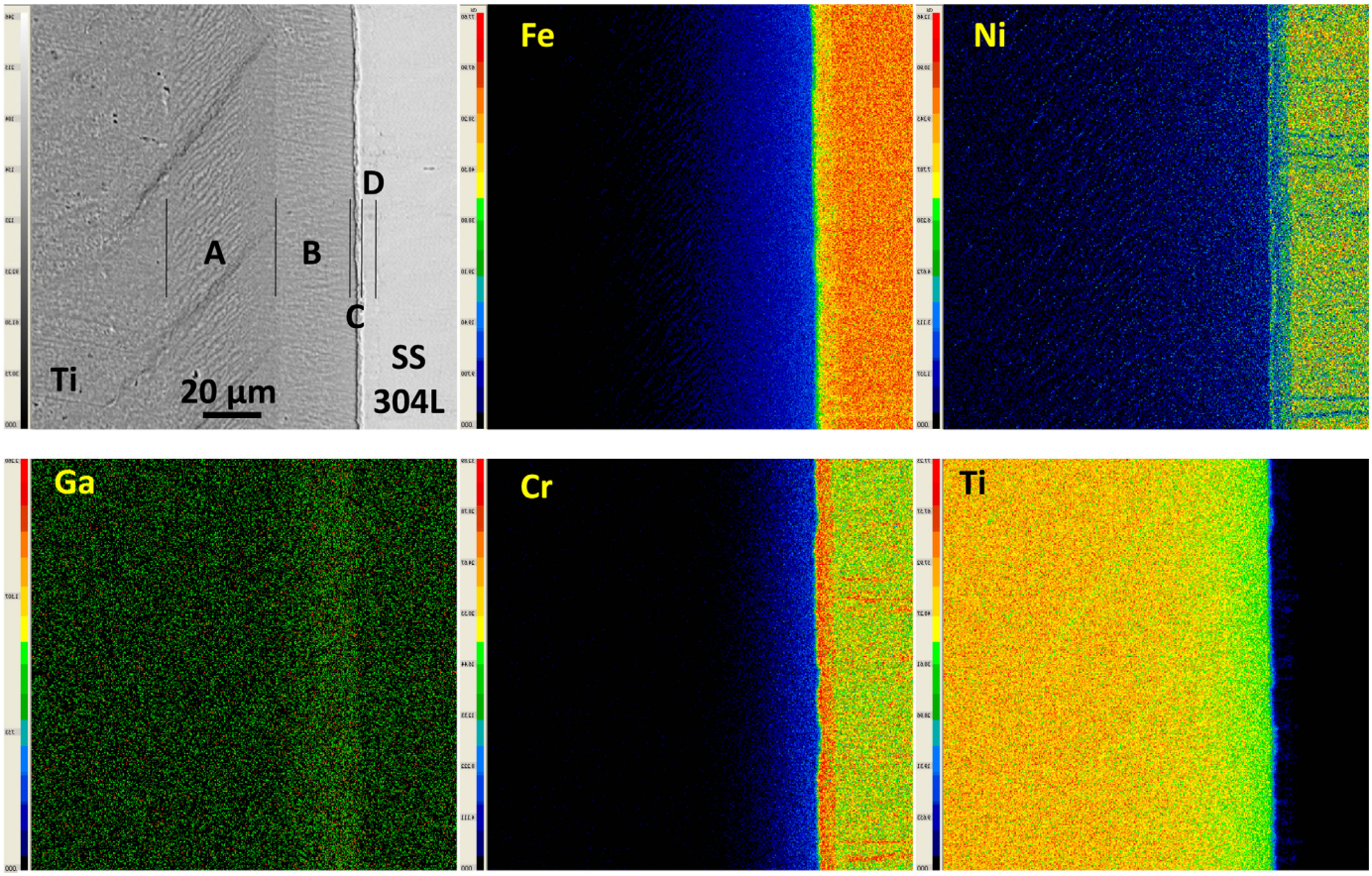


**Fig. 4.** Back scatter SEM image and elemental maps of a Ti-SS sample bonded at 1050 °C for 20 min.

consists of αFe due to containing two α-stabilising elements, i.e. up to 5 at.% Ga and 22 at.% Cr.

Further examination of specimens from the inter-diffusion zones at finer length scale in TEM revealed detailed features in the interaction zones. Fig. 5 shows a typical high annular angular dark field (HAADF) image of entire region "C" along with the elemental distribution in that region. Clearly, Fe and Ti were spread in the entire region "C", whereas Cr was confined mainly to the region "D" on the steel side. Ti map shows strong tendency of partitioning in one of the phases where presence of Fe is nearly negligible. In order to determine chemical composition of various phases formed in this region, spot analysis with small beam size (~1 nm) was used in order to confine the interaction volume to the individual phases. Table 4 shows the chemical composition of various phases marked 1 to 8 in Fig. 5.

Based on the chemical analysis of various regions seen in HAADF image, the entire region "C" consisted of FeTi and also $(FeCr)_2Ti$, as seen in the bright field micrograph in Fig. 6. The polycrystalline nature of both these intermetallic compounds is clearly revealed in the corresponding micrograph. It was further noticed that the FeTi layer contained fine precipitates with irregular shapes, marked by arrows in Fig. 6, whereas $(Fe,Cr)_2Ti$ appears as a continuous single-phase layer. It is interesting to note that the precipitates within the FeTi layer, shown by white arrow in Fig. 6, proved to be pure Ti. The selected area electron diffraction (SAED) patterns in the region "C" were indexed as αTi and αFe in

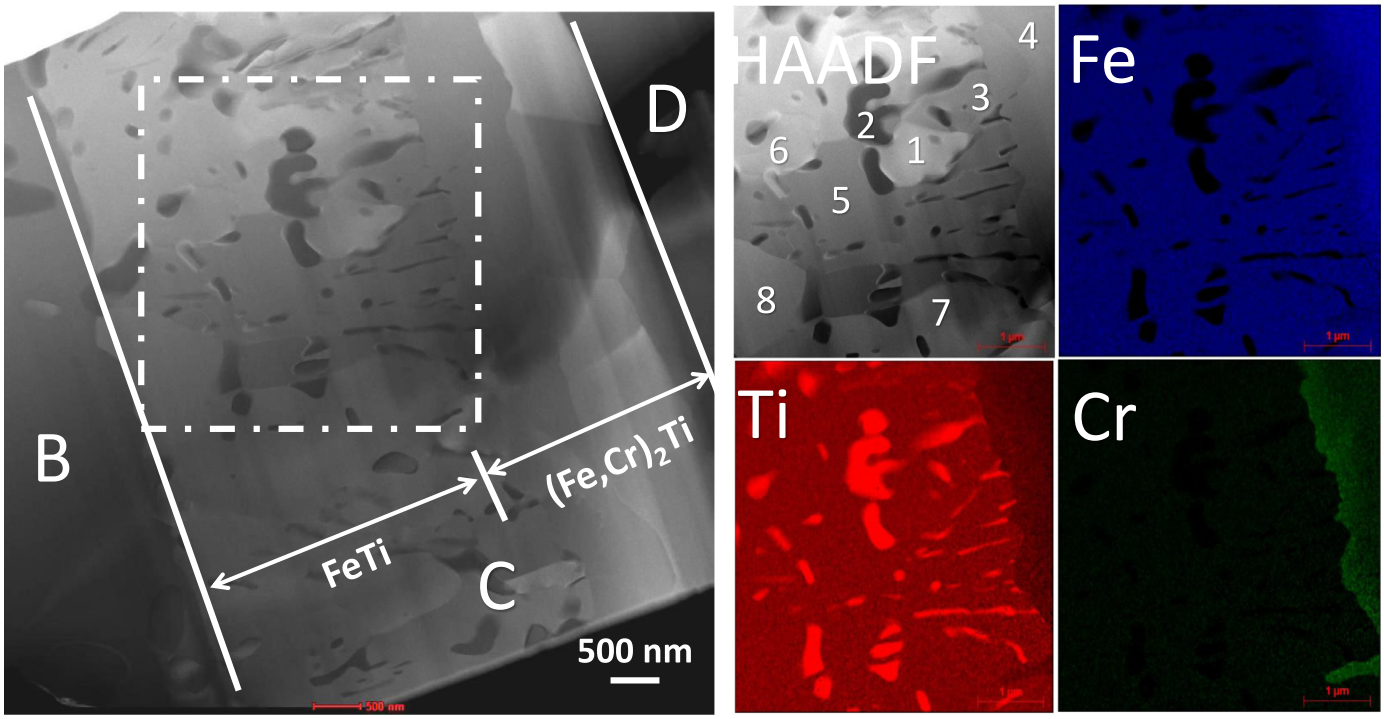


**Fig. 5.** HAADF image of the zone "C" in Fig. 3 along with the X-ray maps of Fe, Ti and Cr acquired by EDS in STEM mode.

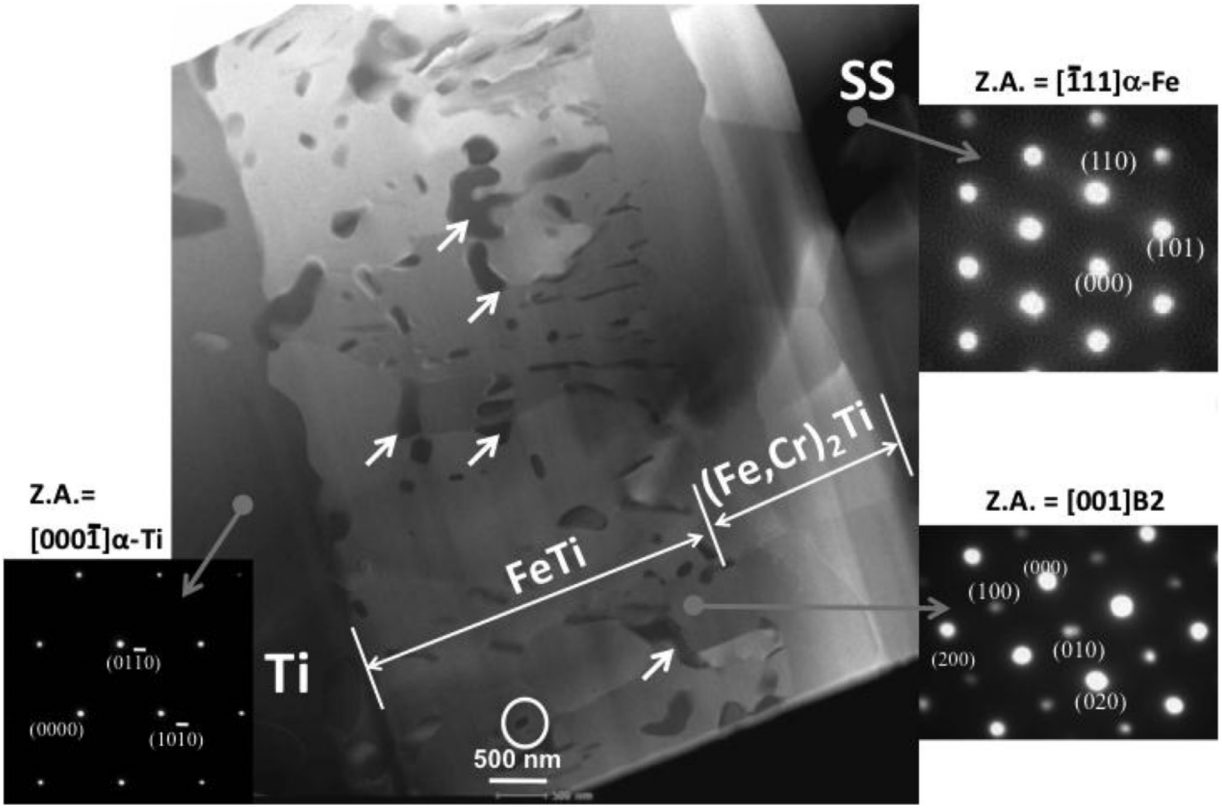


**Fig. 6.** Bright field TEM micrograph showing the intermetallic compounds formed at the SS-Ti interface in a sample bonded at 1020 °C for 20 min. SAED patterns from different regions are also shown.

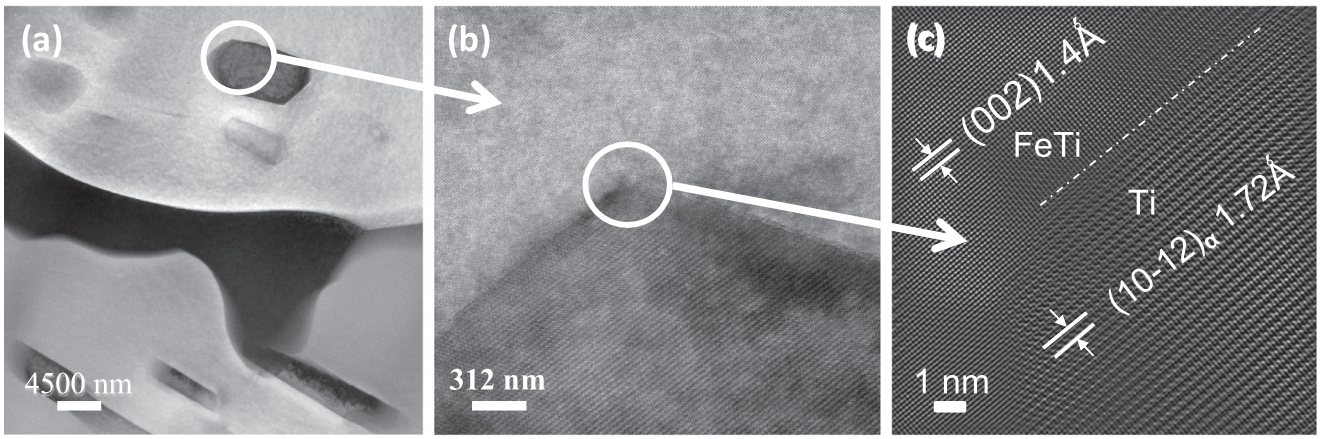


**Fig. 7.** High Annular Angular Dark Field (HAADF) micrograph (a) of the encircled precipitate seen in Fig. 6. High Resolution Scanning Transmission Electron Microscopy (HRSTEM) micrographs (b) & (c) show the nature of the interface between the precipitate and the matrix.

**Table 4**
Chemical composition (at.%) of various locations marked in Fig. 5.

| Locations | Ti | Fe | Cr | Ni | Ga |
|---|---|---|---|---|---|
| 1 | 50.45 | 36.24 | 3.51 | 5.42 | 0.46 |
| 2 | 99.07 | 0.53 | 0.06 | 0.13 | 0.21 |
| 3 | 39.17 | 40.57 | 18.06 | 1.97 | 0.23 |
| 4 | 28.21 | 56.10 | 10.93 | 4.64 | 0.11 |
| 5 | 52.46 | 37.36 | 3.54 | 5.86 | 0.78 |
| 6 | 53.01 | 36.84 | 3.33 | 6.00 | 0.82 |
| 7 | 50.68 | 39.50 | 3.59 | 5.78 | 0.45 |
| 8 | 53.3 | 36.41 | 3.51 | 5.91 | 0.88 |

Fig. 6. The indexed SAED patterns from the FeTi layer on the Ti side, show strong reflections from (020) and (200) and weak superlattice reflections from the (100) and (010) planes.

In order to understand the nature of fine precipitates within the FeTi matrix, further examination at higher magnifications was carried out. As a result, these precipitates were divided into two categories: ones which formed at the grain boundaries having irregular shapes and relatively larger in dimensions, and others within the grains with faceted morphologies. A magnified TEM micrograph of the FeTi layer, encircled in Fig. 6, is shown in Fig. 7a. The faceted nature of the precipitate is evident in this micrograph. Fig. 7b and 7c show the micrographs taken by high resolution scanning transmission electron microscopy (HRSTEM) of the interfacial area between the matrix and precipitate. It appears the faceted sides of the precipitate are coherent with the matrix, suggesting the presence of an orientation relationship.

### 3.2. Microstructural examination of bonds with Ni interlayer

In the case where Ni interlayer was used between SS and Ti, evolution of the microstructure looked quite different from the direct bonded samples without any interlayer. However, the joint interfaces, same as in these direct bonded samples, were free from pores and discontinuities with very similar microstructures regardless of the bonding conditions. Fig. 8 shows typical microstructures of the SS-Ti samples diffusion bonded at 900 and 850 °C for 60 min. The microstructures in both cases seem to be similar, where, the SS side remains nearly unaffected and almost the entire reaction zone is confined to the Ti side. The widths of the interaction zones were about 80 μm and 200 μm for the samples bonded for 60 min at 850 and 900 °C, respectively. Such a sharp increase in the width of the reaction zone may be attributed to the $\alpha$-$\beta$ transition in Ti which occurs at 882 °C.

Based on morphological variation, the reaction zone was divided into three distinct regions marked as “E”, “F” and “G” in Fig. 8. A magnified view of the thin region “E” in the sample made at 850 °C and the corresponding concentration profiles are shown in Fig. 9. The entire width of the region “E” at this bonding condition was found to be only about 2 μm. It is evident from the corresponding FESEM micrograph that the region “E” consisted of three distinct layers, as marked in Fig. 9. These layers were identified as a Cr enriched $\alpha$Fe with a width of about 1μm, a thin layer of $Fe_2Ti$ in the middle and a B2 compound (Fe,Ni)Ti on the titanium side. EDS-TEM analysis was also carried out at 3 points on the region “E”. One of the points, coincided with the (Fe,Ni)Ti phase, contains 62.8 at.% Ti, 21.3 at.% Fe, 2.0% Cr, 13.9 at.% Ni. Two other points were in $\alpha$Fe layer with a composition of 58.5% Fe, 34.5% Cr, 4% Ni and 3% Ti. It can be seen that the compositions that were determined using EDS in TEM matched closely with those determined using EDS in SEM (shown in Fig. 9). The graph in Fig. 9 shows about 30 at.% enrichment of Cr and 5 at.% depletion of Ni in the $\alpha$Fe. Such high concentration of Cr, an $\alpha$Fe stabilizer, and depletion of Ni, a $\gamma$Fe stabilizer, led to the formation of the 1μm thick $\alpha$Fe phase. About 10 at.% Cr was also found to exist in the $Fe_2Ti$ phase. Kessler et al. [29] reported a large solubility of Cr in the phase $Fe_2Ti$. Hence this phase may be denoted as $(Fe,Cr)_2Ti$. It must be noted that both $Fe_2Ti$ and $Cr_2Ti$ phases have the same crystal structure i.e. C14 (hP12).

The distribution of different elements in the inter-diffusion zone in the sample bonded formed at 900 °C for 60 min have been shown using X-ray maps of the individual elements in Fig. 10. A close examination of the X-ray maps of Cr in Fig. 10 indicated a slight enrichment of Cr at the interface, due to the formation of the $\alpha$Fe(Cr) and $(Fe,Cr)_2Ti$ phases in the region “E”. The observation of Cr enrichment of about 30 at.% at the interface in X-ray map is corroborated by the concentration profile shown in Fig. 9. The FeTi phase layer formed at the interface contained about 12 at.% Ni and about 4 at.% Cr apart from Fe and Ti. It is worth mentioning that both the binary systems Fe-Ti and Ni-Ti contain B2 phases FeTi and NiTi, respectively. Interestingly, the Fe-Ni-Ti phase diagram, shown in Fig. 11, exhibits a complete solubility range of these two compounds, and hence can be denoted as (Fe,Ni)Ti. Therefore, it can be inferred that in the present case, the (Fe,Ni)Ti phase formed at the interface due to inter-diffusion of Fe, Ni and Ti.

The X-ray map of Ga showed that a small quantity of Ga remained in the diffusion zone. The X-ray maps of Fe, Ni and Cr in Fig. 10 also depicted diffusion of these elements into Ti. However, the penetration depths of Fe and Ni were much deeper than that of Ga and Cr. As indicated earlier, a two-phase layer “G” formed due to the diffusion of mainly Ni and Fe into Ti. During bonding at temperatures above the $\alpha$-$\beta$ transus, only $\beta$Ti exists but during the subsequent cooling, it transforms

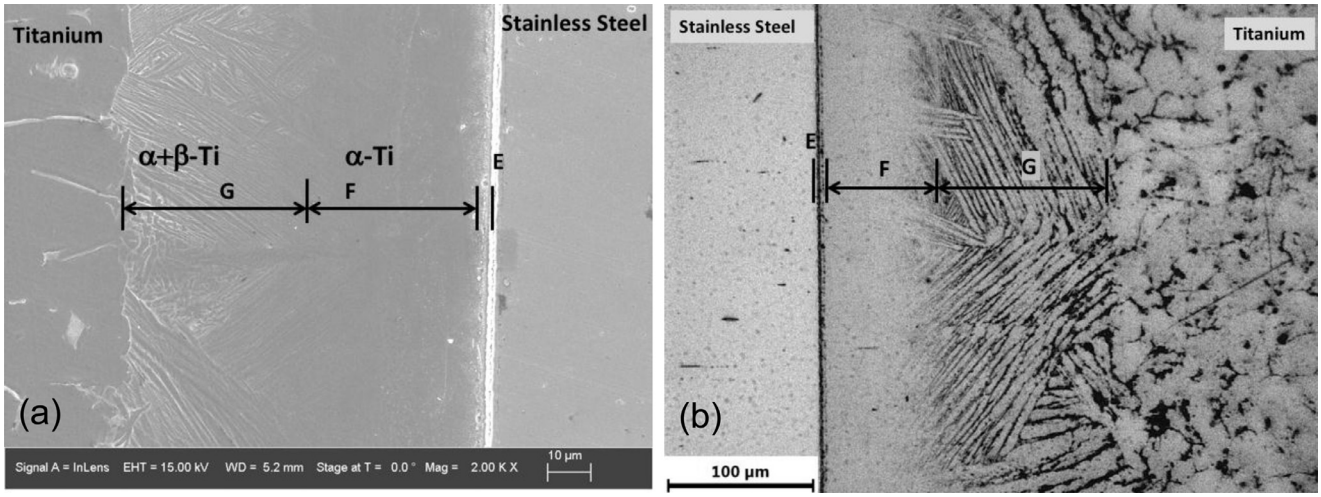


**Fig. 8.** Optical micrograph of the SS-Ti interface in samples bonded at 850 °C (a) and 900 °C (b) for 60 using Ni interlayer.

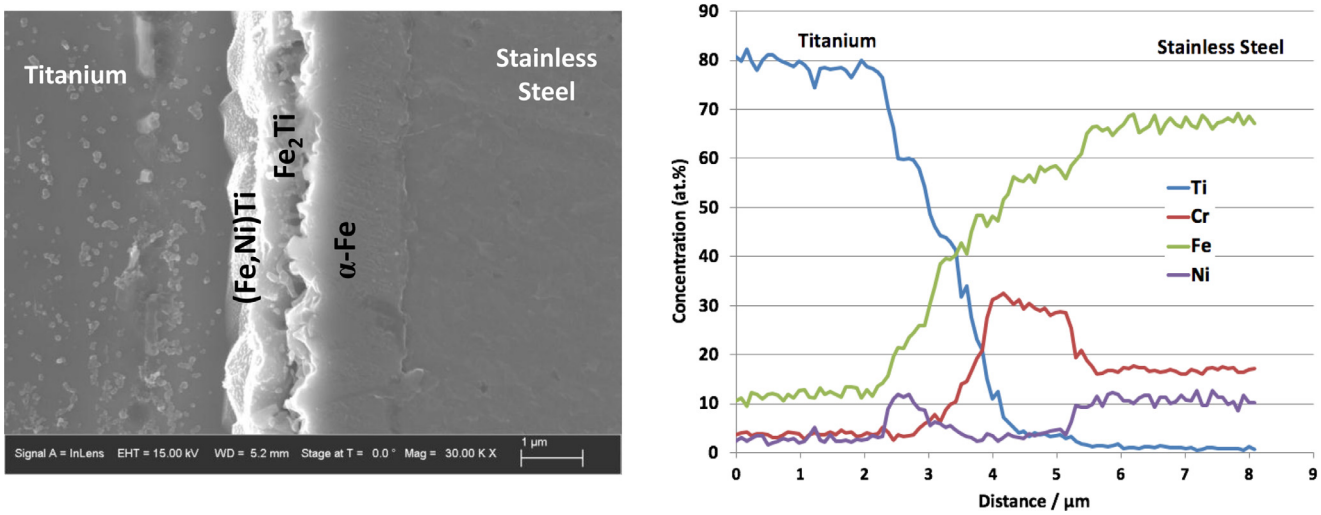


**Fig. 9.** FESEM micrograph of the SS-Ti interface in a sample bonded at 850 °C for 60 min with Ni interlayer and the corresponding concentration profiles of main elements.

to $\alpha + \beta$ phases in region "G". Since both Ni and Fe are $\beta$-stabilising and have higher solubility in $\beta$Ti compared to $\alpha$Ti, they preferentially are partitioned into the $\beta$Ti phase (see Fig. 10). Therefore, it is reasonable to assume that cooling at a moderately high rate (as in the present case), the $\beta$Ti in the region "G" transformed by nucleation of different variants of $\alpha$Ti. These nuclei then grew to form acicular shaped plates in different directions to ultimately produce a basket weave Widmanstatten structure. Fig. 12 shows a HAADF image and the X-ray maps of main elements of the inter-diffusion zone in a joint bonded with Ni interlayer at 820 °C for 2 h.

The X-ray map of Ga clearly shows that the interaction zone contained negligible amount of Ga. This is anyway expected since Ga has a much higher solubility in $\alpha$Ti. Two IMC layers, *viz.* (Fe,Ni)Ti and $(Fe,Cr)_2Ti$ could be identified (marked on Fig. 12) based on their compositions in the X-ray maps. Also, a 1 µm thick layer of $\alpha$Fe, containing high amount of Cr, formed on the SS side of the intermetallic compounds.

### 3.3. Variation in hardness

The variation in the hardness across the inter-diffusion zone in SS-Ti joints was evaluated using the nano-hardness indentation technique. Fig. 13 shows the hardness profiles across the interface in the samples bonded at 850 °C for 30 min and 850 °C for 120 min with Ni interlayer. The slight drop in hardness at 20 µm is within the statistical variation in the hardness values, or due to the indentation falling on a local defect in the sample. The hardness increased from about 3.9 GPa in the stainless steel to about 5.0 GPa in the inter-diffusion zone and dropped again to about 2.6 GPa on the Ti-side of the sample bonded at 850 °C for 30 min. A similar trend was also observed in the case of the joints bonded at 850 °C for 120 min with Ni interlayer. The intermediate increase in hardness values could be attributed to the formation of the intermetallic compounds at the interface. The inter-diffusion of Fe, and Ni, to some extent, also increased the hardness of Ti.

### 3.4. Bond strength and fracture behaviour

Fig. 14 shows the results of the tensile tests performed on SS-Ti joints, bonded with and without Ni interlayers. The maximum strength obtained was 280 MPa, for the joint bonded at 850 °C for 60 min using a Ni interlayer. The SEM fractographs taken of the tensile-tested sample are shown in Fig. 15. It could be seen that the failure took place primarily in brittle mode. However, some evidences of ductile failure were observed in certain locations, marked by circles in Fig. 15. Further optimisation of the gallium-assisted bonding without Ni interlayer resulted in a higher bond strength of 313 MPa which is 92% of the yield strength

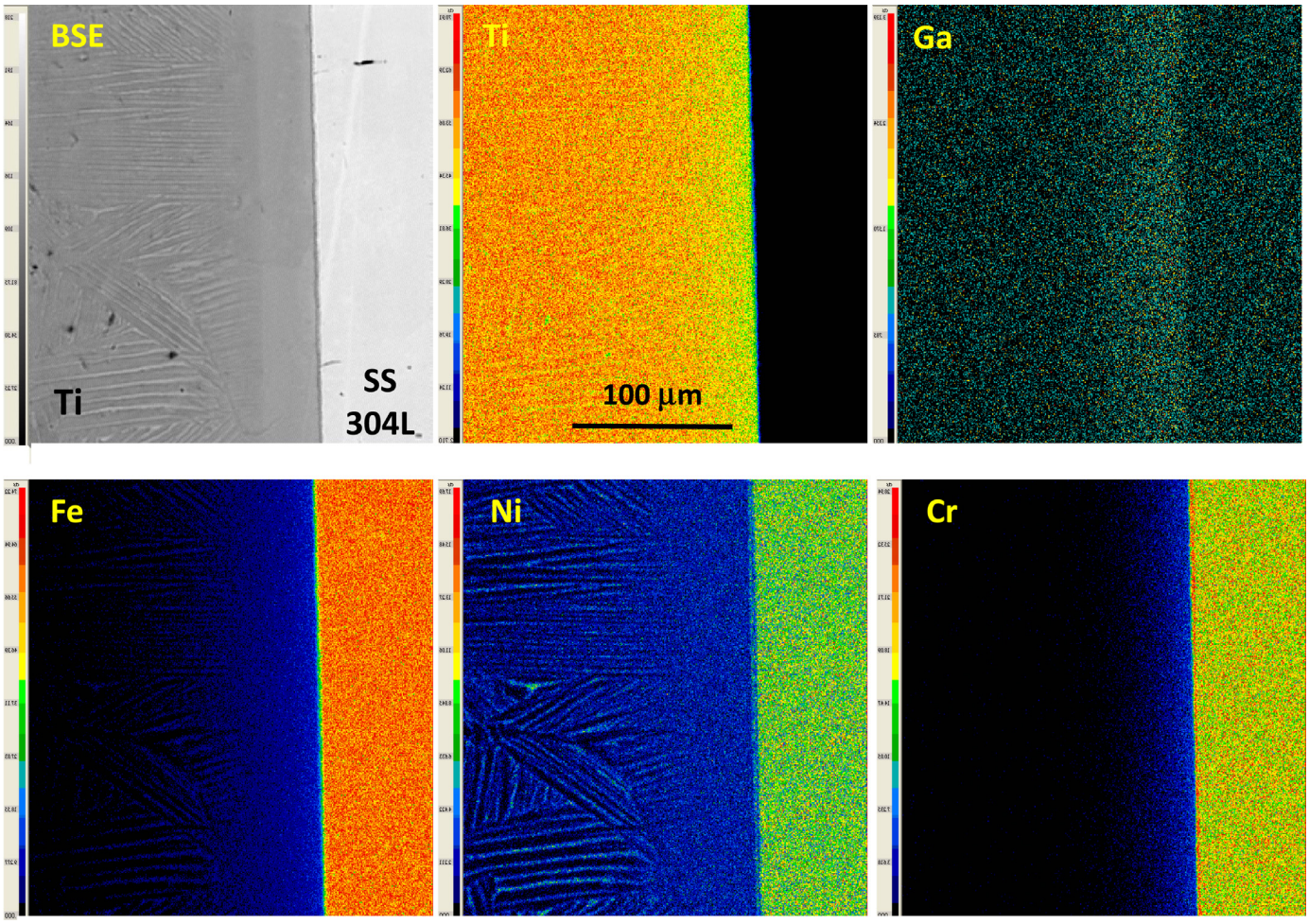


**Fig. 10.** BSE image and X-ray maps of the individual elements Fe, Ni, Cr, Ti and Ga showing their distributions at the SS-Ti interface in a joint bonded at 900 °C for 60 min with Ni interlayer.

of the Ti used in this work. Due to the legal issues related to bonding titanium to stainless steel, further investigation on high strength bonds was not possible.

## 4. Discussion

In the present study, two cases of gallium-assisted diffusion bonding of SS to Ti, one directly without any interlayer and other with a Ni interlayer were studied. The commonality between the two cases, is that the reaction zones are extended more towards the Ti side than the SS side. One possible reason for such behaviour is that the diffusion of Fe and Ni in Ti is much faster than the diffusion of Ti in stainless steel. The activation energies of Fe and Ni in $\beta$Ti are 134 and 123.9 kJ/mol, respectively, as compared to 293.2 kJ/mol for the diffusion of Ti in a Fe matrix [30]. Given the exponential relation between the activation energy and diffusion rate, Fe and Ni can diffuse up to one order of magnitude faster in Ti than Ti in SS.

Upon inter-diffusion of the elements at the joining interface, when the concentration exceeds the solubility limit, the formation of intermetallic phases initiates, e.g. FeTi and $Fe_2Ti$ marked as region "C" in Fig. 3. The first phase to form in the diffusion zone was assumed to be FeTi, owing to its lower Gibbs free energy of formation ($\Delta G^0 = -20.109$ kJ/mol for FeTi and $-17.745$ kJ/mol for $Fe_2Ti$) [31]. Subsequently, $Fe_2Ti$ forms at the newly formed FeTi and $\alpha$Fe interface. Meanwhile, in the region "B", the diffusion of Ga led to formation of $\alpha$Ti on the Ti side due to its strong $\alpha$stabilising effect. Upon cooling from the bonding temperatures, in the regions where Fe and Ni have sufficiently diffused, a duplex microstructure of $\alpha+\beta$ Ti formed on the Ti-side (marked as "A" in Fig. 3). The formation of Ti-rich precipitates within the FeTi phase, comprising a two-phase microstructure, in the diffusion zone of the direct bonded samples is an interesting observation. A close examination of the Fe-Ti phase diagram in Fig. 16 revealed that the solubility range of the FeTi phase is asymmetric at about the 50 at.% line. The phase field of FeTi phase in the Fe-Ti phase diagram also shows the solubility of Ti is more than that of Fe in FeTi. In addition, the solubility of Ti in off-stoichiometric FeTi reduces at lower temperatures ($T < 1065$ °C). Therefore, during the process of cooling of the bonded couple, the excess Ti was rejected from the FeTi phase. At temperatures above 595 °C, the excess Ti may precipitate out in form of $\beta$Ti(Fe), provided sufficient solubility of Fe exist, while at temperatures below 595 °C it may precipitate out in form of $\alpha$Ti(Fe) with limited solubility. Upon cooling the solubility of Ti decreases, hence any excess Ti comes out of FeTi matrix, thereby forming Ti precipitates. In other words, since no other intermetallic could form with a Ti concentration higher than in FeTi, any excess Ti would remain unreacted. In order to ascertain the mode of microstructural evolution, the interfacial region was examined in detail using HRSTEM.

Microstructural investigations revealed the nucleation of pure Ti precipitates homogeneously in the FeTi matrix. The size of these Ti precipitates varied from 100 nm to about 500 nm. The shape of these precipitates also varied considerably, i.e. ranging from almost spherical to very elongated. Had the excess Ti precipitated out at temperatures higher than 595 °C, fine precipitates should have higher concentration of Fe.

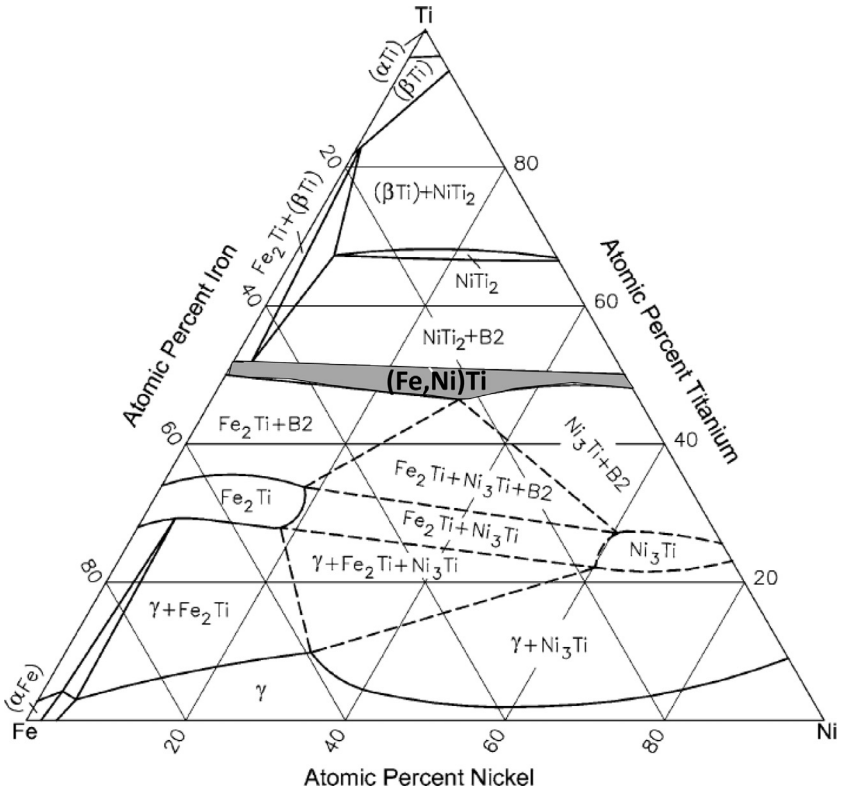


**Fig. 11.** Ternary phase diagram of Fe-Ti-Ni system at 800 °C. The phase field of (Fe,Ni)Ti is highlighted.

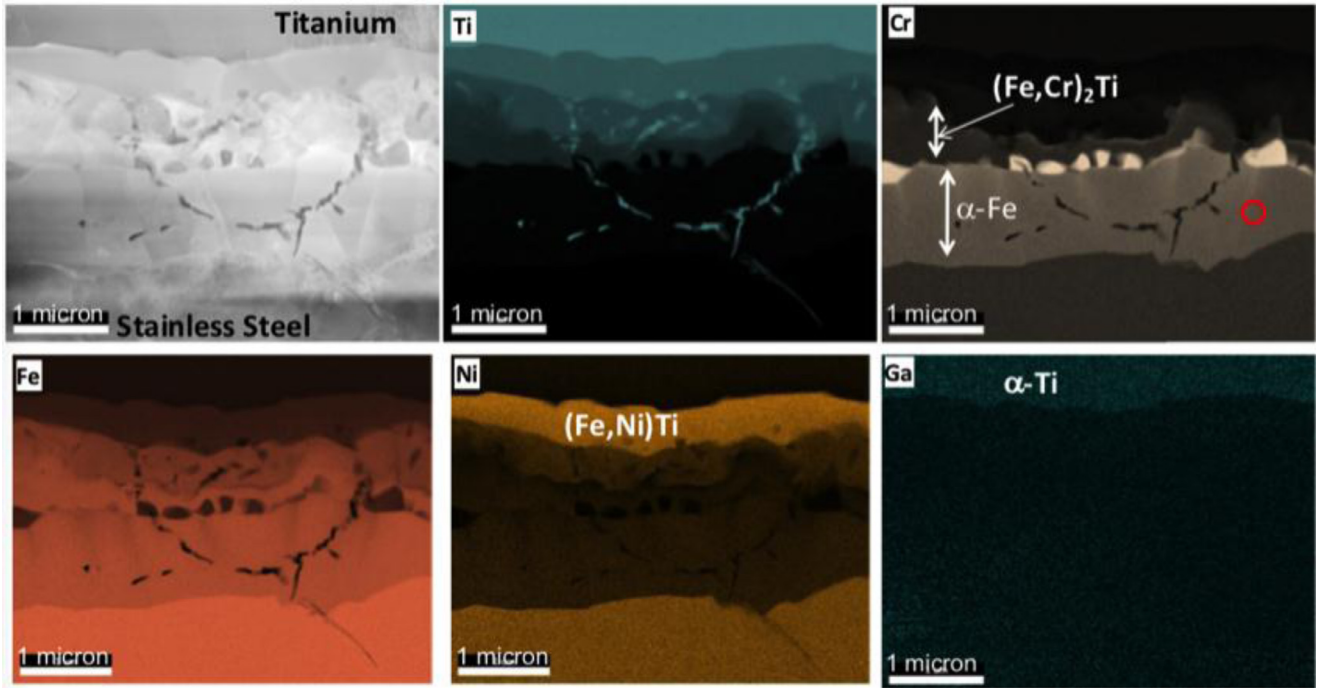


**Fig. 12.** HAADF micrograph along with X-ray maps of Ti, Fe, Ni, Cr and Ga in the inter-diffusion zone of a SS-Ti couple bonded at 820 °C for 2 h with Ni interlayer.

However, compositional analysis showed that the Fe concentration in precipitates is as low as 0.5%. Upon cooling, the high temperature $\beta$ phase would decompose into $\alpha$Ti and FeTi (i.e. eutectoid transformation). Closer examination of the microstructure failed to show formation of any such eutectoid products. Fig. 7a, in fact, shows monolithic form of precipitates ruling out any possibility of the eutectoid transformation. Formation of precipitates at the grain boundaries and within the grains, suggested that the precipitation process occurred in two steps. Precipitation at the grain boundaries required long range diffusion of Ti and hence could occur at relatively high temperatures. The remaining excess Ti precipitated at lower temperature within the grains. The Ti precipitates on the grain boundaries did not have any crystallographic

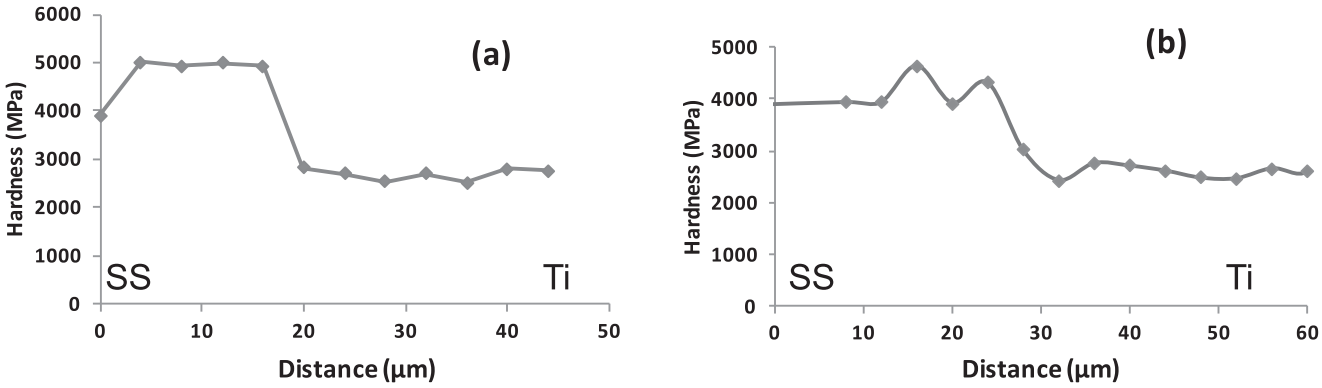


**Fig. 13.** Variation in nano-hardness across the inter-diffusion zone of SS-Ti joints diffusion bonded at (a) 850 °C for 30 min and (b) 850 °C for 120 min both with Ni interlayer.

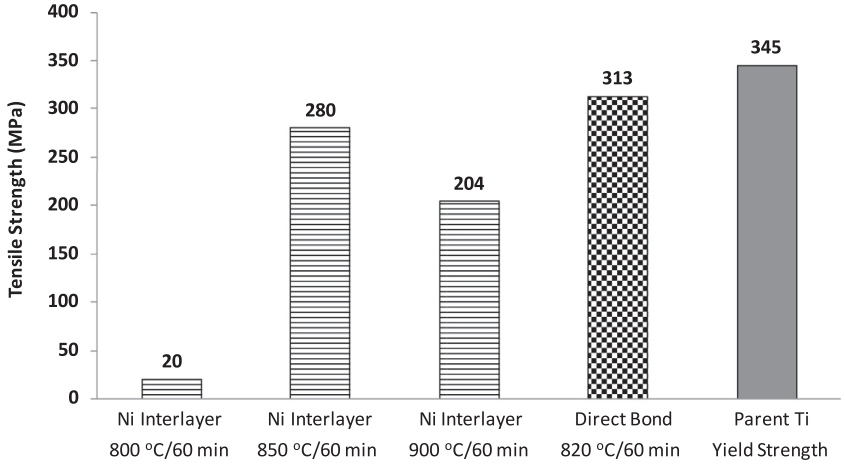


**Fig. 14.** Tensile strength of SS-Ti samples, made using gallium-assisted diffusion bonding, compared to the yield strength of un-bonded parent Ti-G2.

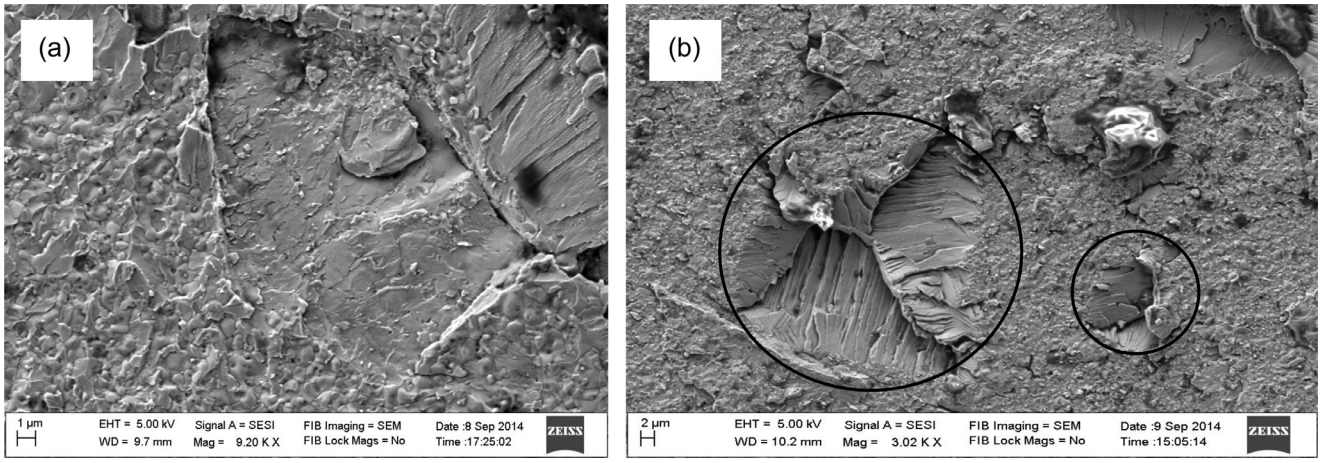


**Fig. 15.** Fractographs from steel side (a) and titanium side (b) of a sample, bonded at 850 °C for 60 min, show the presence of limited ductility.

relationship with the matrix phase. On the other hand, those within the grains showed Burger orientation relationship with the matrix phase (0001) $\alpha//(110)_{FeTi}$ and $<11\text{–}20>\alpha//<111>$ FeTi. The matching planes (see Fig. 7c) and the orientation relationship between the matrix and the precipitates both support the likelihood of strain energy minimization during the precipitation process. The X-ray maps of Fig. 12 showed enrichment of Cr in the $Fe_2Ti$ phase to a large extent.

In the case of bonding with Ni-interlayer, the width of the interaction zone, increases from 80 to 200 μm, when the bonding temperature was increased from 850 to 900 °C both with the same bonding time of 60 min. This sharp increase in the width could be attributed to the $\alpha$-$\beta$ lattice transition from HCP, a close packed structure, to BCC, which is an open structure. It also could be due to the fact that the activation energy for diffusion of Ni in $\alpha$Ti is higher than that in $\beta$Ti phase (139.5 compared to 123.9 kJ/mol) [30].

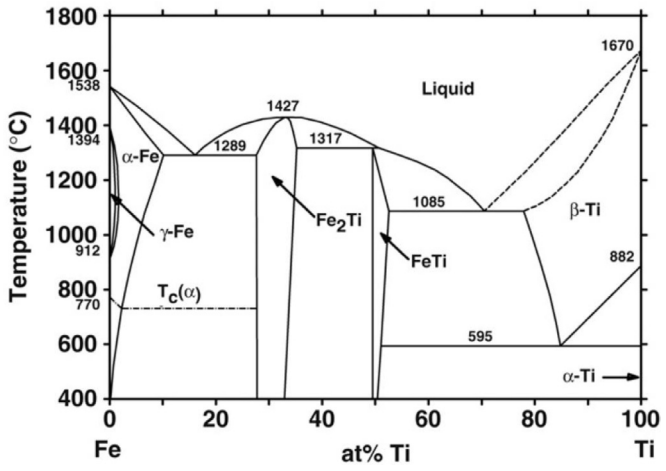


**Fig. 16.** Phase diagram of Ti–Fe (courtesy of J.L. Murray, Phase Diagrams of Binary Titanium Alloys, ASM International, 1987, pp. 99111).

One of the interesting observations was the formation of the $\beta$Ti phase in the inter-diffusion zone even at bonding temperatures below the $\alpha$-$\beta$ transition temperature. For example, the formation of the two-phase $\alpha+\beta$ layer in the sample bonded at 850 °C (Fig. 8), clearly revealed that $\beta$Ti phase could form well below the $\alpha$–$\beta$ transition temperature. This could be attributed to the diffusion of the $\beta$-stabilising elements, like Fe and Ni into Ti. However, the bulk of Ti maintained its $\alpha$ structure. During subsequent cooling, the high temperature $\beta$Ti phase decomposed to a mixture of $\alpha$Ti and $\beta$Ti as a result of the expected eutectoid transformation. This explains the formation of $\alpha+\beta$ phase mixture (region "G" in Fig. 8) even if the bonding temperature was below the $\alpha$-$\beta$ transition temperature, *viz.* 800 °C, 820 °C and 850 °C.

Depending on the nature of the alloy system and the cooling rate, $\beta$Ti phase may either transform to $\alpha+\beta$ structure or decompose to $\alpha$Ti and an intermetallic compound [32]. The latter case is termed as "active eutectoid decomposition", which is prevalent in certain systems with high eutectoid temperatures and low solute concentrations [33]. It is interesting to note that the Ti-Ni system exhibited active eutectoid decomposition, whereas Ti-Fe system had a normal eutectoid reaction. This is because the eutectoid temperature is higher in the former than in the latter (765 °C compared to 595 °C). In this work, the region "G" in Fig. 8 consisted of $\beta$Ti(Ni,Fe) solid solution, which underwent decomposition upon cooling. However, due to the presence of Fe alongside Ni, the tendency for active eutectoid transformation was suppressed. This explains the fact that in spite of the presence of large quantity of Ni in the region "G", the microstructure of this region showed $\alpha+\beta$ structure and not a eutectoid transformed structure, as may be expected of a binary Ti-Ni system.

## 5. Conclusions

The main conclusions that can be drawn from the present study are as follows:

1- A methodology for preparing strong joints between stainless steel (SS 304L) and pure titanium (grade 2) with tensile strength up to 313 MPa was developed using a novel technique which relies on a pre-bonding surface modification using gallium.
2- Layers of FeTi and $(Fe,Cr)_2Ti$ intermetallic compounds formed at the inter-diffusion zone in the case of direct bonding, and (Fe,Ni)Ti and $Fe_2Ti$ in the presence of nickel interlayer.
3- A layer of $\alpha$Fe was stabilised on the stainless side of the intermetallic layers in all cases, due to the enrichment of chromium at the interface. On the Ti side, the diffusion of gallium led to formation of a layer of $\alpha$Ti, while the diffusion of Fe and Ni helped in stabilizing the $\beta$-Ti phase which later decomposed to a $\alpha+\beta$ Ti structure upon cooling.
4- Although the primary mode of failure of the joints seemed to be through the layers of intermetallic compound layers, and brittle in nature, signs of some ductile failure were also observed.

## Declarations of interest

none

## Acknowledgements

The project was supported by the UK Research Councils (EPSRC) and the Department of Atomic Energy of India. The help received from Dr. Babu Viswanathan for conducting transmission electron microscopy, and the constant support provided by Prof. Hamish Fraser both from Ohio State University are highly appreciated. The first author is grateful for the support received from Guangdong Innovative and Entrepreneurial Research Team Program (Project No. 2016ZT06G025).

## References

[1] K. Martinsen, S.J. Hu, B.E. Carlson, Joining of dissimilar materials, CIRP Ann. Manuf. Technol. 64 (2015) 679–699.
[2] F.C. Campbell, Joining: Understanding the Basics, ASM International, Materials Park, OH, 2011.
[3] A. Laik, A.A. Shirzadi, G. Sharma, R. Tewari, T. Jayakumar, G.K. Dey, Microstructure and interfacial reactions during vacuum brazing of stainless steel to titanium using Ag-28 pct Cu alloy, Metall. Mater. Trans. A 46A (2015) 771–782.
[4] M.M. Cheepu, V. Muthupandi, S. Loganathan, Friction welding of titanium to 304 stainless steel with electroplated nickel interlayer, Mater. Sci. Forum 710 (2012) 620–625.
[5] A. Fuji, T.H. North, K. Ameyama, M. Futamata, Improving tensile strength and bend ductility of titanium/AISI 304L stainless steel friction welds, Mater. Sci. Technol. 8 (1992) 219–235.
[6] U.K. Mudali, B.M.A. Rao, K. Shanmugam, R. Natarajan, B. Raj, Corrosion and microstructural aspects of dissimilar joints of titanium and type 304L stainless steel, J. Nucl. Mater. 321 (2003) 40–48.
[7] B. Raj, U.K. Mudali, Materials development and corrosion problems in nuclear fuel reprocessing plants, Prog. Nucl. Energy 48 (2006) 283–313.
[8] M.M. Schwartz, Brazing, ASM International, Materials Park, OH, 2003.
[9] A. Laik, A.A. Shirzadi, R. Tewari, A. Kumar, T. Jayakumar, G.K. Dey, Microstructure and interfacial reactions during active metal brazing of stainless steel to titanium, Metall. Mater. Trans. A 44A (2013) 2212–2215.
[10] A. Elrefaey, W. Tillmann, Characterization of titanium/steel joints brazed in vacuum, Weld. J. 87 (2008) 113s–118s.
[11] N. Kahraman, B. Gulenc, F. Findik, Joining of titanium/stainless steel by explosive welding and effect on interface, J. Mater. Proc. Technol. 169 (2005) 127–133.
[12] A. Nobili, T. Masri, M.C. Lafont, Recent developments in characterization of a titanium-steel explosion bond interface, in: W. Chang (Ed.), Proceedings of the Reactive Metals in Corrosive Applications Conference, Albany, OR, 1999, pp. 89–98.
[13] H. Akbulut, O.T. Inal, C.A. Zimmerly, Ion nitriding of explosively clad titanium/steel tandems, J. Mater. Sci. 34 (1999) 1641–1652.
[14] P. Manikandan, K. Hokamoto, A.A. Deribas, K. Raghukandan, R. Tomoshige, Explosive welding of titanium/stainless steel by controlling energetic conditions, Mater. Trans. 47 (2006) 2049–2055.
[15] B. Sabirov, J. Budagov, A. Sissakian, G. Shirkov, Y. Taran, G. Trubnikov, N. Dhanarai, M. Foley, E. Harms, D. Mitchell, S. Nagaitsev, W. Soyars, V. Rybakov, Y. Samarokov, Z. Zhigalov, A. Basti, and F. Bedeschi, 'Recent advances in Ti and Nb explosion welding with stainless steel for 2K operating (ILC Program), in: Proceedings of the of LCWS11′ 2012, arXiv:1201.3472v1 [physics.insdet].
[16] H. Kato, S. Abe, T. Tomizawa, Interfacial structure and mechanical properties of steel-Ni and steel-Ti diffusion bonds, J. Mater. Sci. 32 (1997) 5225–5232.
[17] P. He, J. Jhang, R. Zhou, X. Li, Diffusion bonding technology of a titanium alloy to a stainless steel with a Ni interlayer, Mater. Charact. 43 (1999) 287–292.
[18] G.B. Kale, R.V. Patil, P.S. Gawde, Interdiffusion studies in titanium-304 stainless steel system, J. Nucl. Mater. 257 (1998) 44–50.
[19] G.B. Kale, S.K. Khera, G.P. Tiwari, Interdiffusion in titanium-iron system, Trans. Ind. Inst. Met. 29 (1976) 550–557.
[20] M. Ghosh, S. Chatterjee, Diffusion bonded transition joints of titanium to stainless steel with improved properties, Mater. Sci. Eng. A 358 (2003) 152–158.
[21] S. Kundu, S. Chatterjee, Interfacial microstructure and mechanical properties of the diffusion bonded joints of titanium to stainless steel with nickel interlayer, Mater. Sci. Eng. A 425 (2006) 107–113.
[22] Y. Deng, G. Sheng, C. Xu, Evaluation of the microstructure and mechanical properties of diffusion bonded joints of titanium to stainless steel with a pure silver interlayer, Mater. Des. 46 (2013) 84–87.

[23] S. Kundu, M. Ghosh, A. Laik, K. Bhanumurthy, G.B. Kale, S Chatterjee, Diffusion bonding between commercially pure titanium and 304 stainless steel using copper interlayer, Mater. Sci. Eng. A 407 (2005) 154–160.
[24] S. Kundu, S. Chatterjee, Interface microstructure and strength properties of diffusion bonded joints of titanium–Al interlayer–18Cr–8Ni stainless steel, Mater. Sci. Eng. A 527 (2010) 2714–2719.
[25] N. Orhan, M. Askoy, M. Eroglu, A new model for diffusion bonding and its application to duplex alloys, Mater. Sci. Eng. A 271 (1-2) (1999) 458–468.
[26] A.A. Shirzadi, E.R. Wallach, New method to diffusion bond superalloys, Sci. Technol. Weld. Join. 9 (1) (2004) 37–40.
[27] A.A. Shirzadi, R. Wallach, "Surface treatment of oxidising materials", USA Patent 6669534 B2 (2003) & UK Patent 2380491 (2002).
[28] H. Okamoto, Ga-Ti (Gallium-Titanium), J. Phase Equil. Diffus. 26 (4) (2005) 398.
[29] H.D. Kessler, W. Rosstoker, R.J. van Thyne, 'Titanium Phase Diagrams', Technical Report 52-335, Illinois Institute of Technology 1953.
[30] G. Neumann, C. Tuijn, Self Diffusion and Impurity Diffusion in Pure Metals, Elsevier, Amsterdam, 2009.
[31] X.H. Wang, Z.D. Zou, S.Y. Qu, S.L. Song, Microstructure and properties of the TiC/Fe-based alloy hardfacing layers, J. Mater. Sci. 40 (2005) 3629–3633.
[32] S. Banerjee, P. Mukhopadhyay, Phase Transformations: Examples from Titanium and Zirconium Alloys, Elsevier, Amsterdam, 2007.
[33] G. Cacciamani, J. De Keyzer, R. Ferro, U.E. Klotz, J. Lacaze, P Wollants, Critical evaluation of the Fe-Ni, Fe-Ti and Fe-Ni-Ti alloy system, Intermetallics 14 (2006) 1312–1325.